scientific reports

Check for updates

OPEN

Superior electroadhesion force with permittivity-engineered bilayer films using electrostatic simulation and machine learning approaches

Seongsoo Park[1], Hongjun Chang[1], Jaehyun Kim[1], Yunki Gwak[2]✉ & Janghyuk Moon[1]✉

Electroadhesive forces are crucial in various applications, including grasping devices, electro-sticky boards, electrostatic levitation, and climbing robots. However, the design of electroadhesive devices relies on speculative or empirical error approaches. Therefore, we present a theoretical model comprising predictive coplanar electrodes and protective layers for analyzing the electrostatic fields between an object and electroadhesive device. The model considers the role of protective layer and the air gap between the electrode surface and the object. To exert a higher electroadhesive force, the higher permeability of the protective layer is required. However, a high permeability of the protective layer is hard to withstand high applied voltage. To overcome this, two materials with different permeabilities were employed as protective layers—a low-permeability inner layer and a high-permeability outer layer—to maintain a high voltage and generate a large electroadhesive force. Because a low-permeability inner layer material was selected, a more permeable outer layer material was considered. A theoretical analysis revealed complex relationships between various design parameters. The impact of key design parameters and working environments on the electroadhesion behavior was further investigated. This study reveals the fundamental principles of electroadhesion and proposes prospective methods to enhance the design of electroadhesive devices for various engineering applications.

Robot- Robot-based manufacturing systems, such as smart factories, require efficient and controllable grippers or actuating systems[1]. Among the various adhesive mechanisms, electroadhesion is the most promising approach for achieving this goal[2,3]. A flexible functionality can also be achieved by using an appropriate substrate material[4,5]. Electroadhesion is the attractive force between the electroadhesive pad and the substrate[6–8]. Applying a few kilovolts generates an electric field which is strong electroadhesive forces through electric polarization[9] Compared with other adhesion mechanisms, this method offers the advantages of ultralow energy consumption, gentle handling, and enhanced adaptability[10–12].

To enhance the electroadhesive force, the pad geometry is optimized based on two factors: (1) thickness and (2) interdigit electrode patterns[13–15]. Several studies have investigated various pad geometries for electroadhesive applications and have demonstrated that the pad geometry is crucial for achieving the maximum electroadhesive force and clamp/unclamp speed[16–18]. In particular, the comb shaped electrode geometry is the most commonly used structure and is one of the electrode shapes that exhibits the greatest strength among various structures[19]. The permeability or dielectric constant of the electrode cover is crucial in determining the electrostatic force[20,21]. However, material design of electrode cover in this area has not received considerable attention. The electric field that passes through the electrode cover affects the electrostatic force, also known as the Maxwell stress, at the object surface[22–24]. A cover with high permeability generates a strong electrostatic force, which enhances the electric field produced by the interdigit electrodes[14,25]. Unfortunately, most studies have used high-permeability insulator materials for electrode covers with low breaking voltages during operation[26–28]. Although a thick electrode cover can avoid voltage shortening between the electrodes and the substrate, it significantly reduces the

[1]Department of Energy Systems Engineering, Chung-Ang University, 84 Heukseok-ro, Dongjak-gu, Seoul 06974, Republic of Korea. [2]Department of Mechanical System Engineering, Kumoh National Institute of Technology, Gyeongbuk 39117, Republic of Korea. ✉email: yunkigwak@gmail.com; jhmoon84@cau.ac.kr

electrostatic force[14,29]. To compensate for these shortcomings, the most recent technology is a bilayer electrode cover design that maximizes electroadhesive force. This bilayer design consists of materials such as polyimide (PI) for the inner layer, which is well known for its high breakdown voltage due to relatively low permittivity and high humidity resistance, and polyurethane (PU) for the outer layer which can lead out superior electroadhesive force due to its high permittivity[30–32]. In an experimental environment, electroadhesive force is affected by various phenomena such as humidity, roughness of each layer, and leakage current[33–35]. Even though the protective layer has low electrical conductivity and acts as an insulating layer, a high applied voltage can cause current flow due to the polarization induced high electric field[33]. Humidity is the main factor that changes the permittivity of materials which affects the accumulation of charge[36]. Furthermore, the conductivity of air (RH > 66%) increases exponentially and sharply when the electric field exceeds a certain level[37]. This can result in corona discharge or leakage current, reducing the electroadhesive force[38]. The roughness of the protective layer and the object also affects the dielectric constant. Increased surface roughness reduces the contact area between the protective layer and the object, which in turn diminishes the electroadhesive force[39]. These conditions, which vary according to the experimental environment, cause discrepancies between the analyzed electroadhesive force in the simulation and the actual experimental values. In this study, we employed a simplified model controlling factors such as humidity, leaking voltage, and break voltage to intuitively evaluate the consistent effect of bilayer permittivities on electroadhesive force. To design an electroadhesion gripper which maximizes electroadhesive force, we analyzed the electrostatic forces of 3000 different gripper configurations by using finite element analysis and 7000 different gripper configurations by using AI, considering eight design variables. Through machine learning techniques, we then optimized the gripper structure to achieve the best possible performance, as shown in Fig. 1a.

Methods

Computational method

The electric field distribution E within a general electrode system can be determined using the following equation:

$$div\, \varepsilon\, grad\varphi = 0, \tag{1}$$

where ε, φ denote the permittivity and the scalar electric potential ($E = -grad\varphi$), respectively. The externally generated volume-charge density was not considered. To obtain numerical solutions to Eq. (1), it is unnecessary to solve for the entire surface where the attraction force F_a occurs. On the contrary, owing to the repetitive pattern of the electrodes, E can be computed for a single segment comprising two electrodes with opposite charges[40].

The electrostatic force F_e exerted on the segment can be calculated from the E distribution as follows:

$$F_e = \oint_s TdS, T = \frac{1}{2}(E \cdot D)I + E \otimes D, \tag{2}$$

where T is the Maxwell stress tensor, D is the dielectric flux density, I is the unit diagonal matrix, and $\otimes$ denotes the dyadic product. Equation (2) can be simplified by assuming parallel interdigital electrodes on attractive object surfaces. The Maxwell stress tensor is expressed as follows:

$$\mathrm{T} = \begin{bmatrix} \frac{\varepsilon}{2}\left(E_x^2 - E_y^2\right) + \frac{1}{2\mu}(B_x^2 - B_y^2) & (\varepsilon E_x E_y + \frac{1}{\mu}B_x B_y + E_x P_y + E_y P_x - B_x M_y - B_y M_x) \\ (\varepsilon E_x E_y + \frac{1}{\mu}B_x B_y + E_x P_y + E_y P_x - B_x M_y - B_y M_x) & \frac{\varepsilon}{2}\left(E_x^2 - E_y^2\right) + \frac{1}{2\mu}(B_x^2 - B_y^2) \end{bmatrix}$$

where E_x and E_y are the electric field components, B_x and B_y are the magnetic field components, P is polarization, and M is magnetization. As we assume our system is electrostatic condition, the B, M is neglected. The P which the function of E and ε is calculated by following equation:

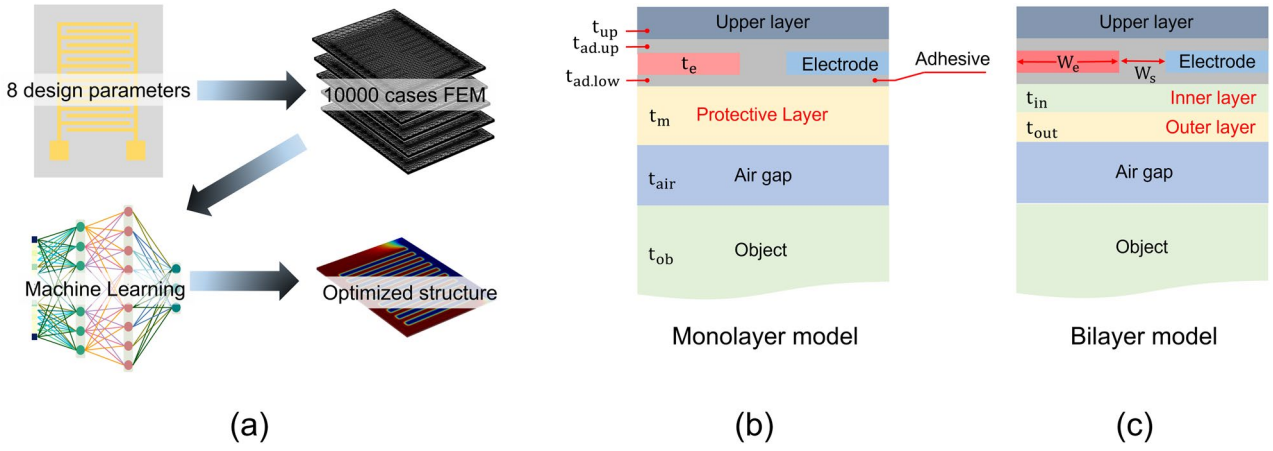

Figure 1. (**a**) Schematic of the interdigitated electrode and the analysis steps, from geometry generation to AI-based optimization. Model structures of interdigitated electrodes with (**b**) a monolayer and (**c**) bilayer protective layer with various dielectric constants. *FEM* finite element method.

$$P = \varepsilon \varepsilon_{relative} E \tag{3}$$

where $\varepsilon_{relative}$ denotes the relative permittivity.

The normal direction of the electrostatic force F_{ey} acting on the segment with electrodes of length = 1 is obtained as

$$F_{ey} = \oint_S T_y dS = \frac{1}{2}\varepsilon l \int_0^{w+g} (E_y^2 - E_x^2) dx. \tag{4}$$

F_{ey} between the two parallel capacitor plates is expressed as

$$F_{ey} = \frac{\partial W_e}{\partial y} = -\frac{1}{2}\frac{\partial E_y D_y}{\partial y} \int_V dV = -\frac{\varepsilon}{2}\left(\frac{U}{t}\right)^2 wl, \tag{5}$$

where W_e, D_y, V are the total energy, the electric displacement field component, and the capacitor volume, respectively. U is the applied voltage, and t is the distance between the electrodes[41].

ML algorithms

We developed an ML model using the RF algorithm, which is known for its ability to process complex and nonlinear data. This ensemble method combines multiple decision trees to improve the prediction accuracy and prevent overfitting[42]. Our dataset comprised 1000 samples calculated through finite element method simulations, covering a wide range of electroadhesive actuator designs. The input features for the model included the voltage, electrode spacing, outer and inner permittivities of the protective layers, air gap, outer and inner thicknesses of the protective layers, and electrode width. These features are critical for determining the electrostatic forces exerted by actuators. We implemented rigorous training and validation procedures, including hyperparameter tuning and cross validation, to ensure the reliability of the model for predicting the effects of these diverse design parameters. In addition, we conducted an in-depth analysis of feature importance, which provided valuable insights into the most important factors that influence electrode design optimization and facilitate the improvement of the electroadhesive actuator performance.

Results

Electric field and force analysis

Figure 1b,c illustrate schematics of the interdigit electrodes used for electroadhesion simulation. The object is separated from the conductive electrodes by a protective layer, which is either a monolayer or a bilayer[43]. These protective layers serve as insulators and have ambiguous breakdown voltage shortages[44,45]. A simulation was conducted under the same applied voltage of 10 kV, disregarding the breaking voltage, to directly compare the electroadhesive force with respect to changes in permittivity between bilayer and monolayer protective layers. It is well-known that insulators with lower permeabilities exhibit higher breaking voltages, and vice versa[25]. The voltage between 1 and 10 kV is applied to one electrode, and it is set to zero (ground) for the other electrode[46,47]. The electric field generated between the two electrodes exerts an adhesive force on various object materials[48–50]. We have assumed that all of the electroadhesive gripping has caused no mechanical damage or chemical reactions. The detailed parameters and material properties are listed in Table 1. Further, the design of the interdigit electrode is analyzed by numerically solving a formulated mathematical model. The electrostatic force is then derived from the electric field distribution and integrated field infectivity on the object surface.

Figure 2a illustrates the electrode potential contours within a single period of the interdigitated electrode configuration. The most distinct potential gradient is observed between the adjacent electrodes, radiating outward in a radial pattern. The permittivity variations between the monolayer and bilayer protective layers profoundly affect the contour slopes. There is not a significant change observed in the voltage gradient which means the electric field along to the x-direction for both monolayer and bilayer structures, while the electric field along to the y-direction shows slightly differences at the outer layer. This electric field change which in turn influence the electrostatic forces exerted on the adhered object.

The electric field distributions across the entire domain and at the object surface are shown in Fig. 2b,c, respectively. The vertical (y-axis) electric field shows the maximum and minimum intensities at the edge of the positively and ground charged electrodes, respectively. Conversely, the horizontal (x-axis) electric field peaks in the interelectrode space and diminishes directly on the electrodes. When using a bilayer protective layer, the y-axis component electric field strength at both edges is observed as 33.57 MV/m which is approximately 1.1% greater compared to the single-layer protective layer (33.15 MV/m), while the x-axis component electric field strength difference is only 0.17%. These results mean that the y-axis component electric field is a factor that increase the electroadhesive force. The components of the Maxwell stress tensor which directly related to the electroadhesive force exhibit maxima at the electrode edges and subsequently taper off along the segment axis to reach a nadir, which in turn induces repulsive forces on the adjacent object. Conventionally, a protective layer with high permittivity may have a lower breakdown voltage. It means that using a protective layer with superior permittivity might not necessarily lead to an increase in electroadhesive force. However, when the bilayer protective layer is adopted, it has been observed that the strength of the electric field is higher in the inner layer than in the outer layer. This implies that the inner layer is a buffer zone for the electric field, leading to electric field shielding. The inner layer's presence can improve the outer layer's breakdown voltage. The bilayer protective layer shows a higher electroadhesive force than a single protective layer at the same voltage, and it is anticipated to demonstrate superior performance when considering breakdown voltage as well. Figure 2d presents a comparison of the electrostatic adhesive forces based on the different permittivity. The results indicate a direct

Description [unit]	Parameter	Value	Min	Max
Electrode width [μm]	W_e	75	50	500
Electrode spacing [μm]	W_s	100	50	500
Upper layer thickness [μm]	t_{up}	25	–	–
Upper adhesive thickness [μm]	$t_{ad.up}$	25	–	–
Electrode thickness [μm]	t_e	35	–	–
Lower adhesive thickness [μm]	$t_{ad.low}$	5	–	–
Monolayer thickness [μm]	t_m	25	–	–
Air thickness [μm]	t_{air}	50	30	150
Object thickness [μm]	t_{ob}	800	–	–
Inner layer thickness [μm]	t_{in}	12.5	10	100
Outer layer thickness [μm]	t_{out}	12.5	10	100
Voltage [kV]	V	10	1	10
Upper layer permittivity	ε_{up}	2	–	–
Adhesive permittivity	ε_{ad}	3.6	–	–
Monolayer permittivity	ε_m	3.5	–	–
Object permittivity	ε_{ob}	2.3	–	–
Inner layer permittivity	ε_{in}	2.5	1	10
Outer layer permittivity	ε_{out}	4.5	1	10
Electrode permittivity	ε_e	1	–	–
Air permittivity	ε_{air}	1	–	–

Table 1. Calculated design parameters and their ranges for finite element analysis.

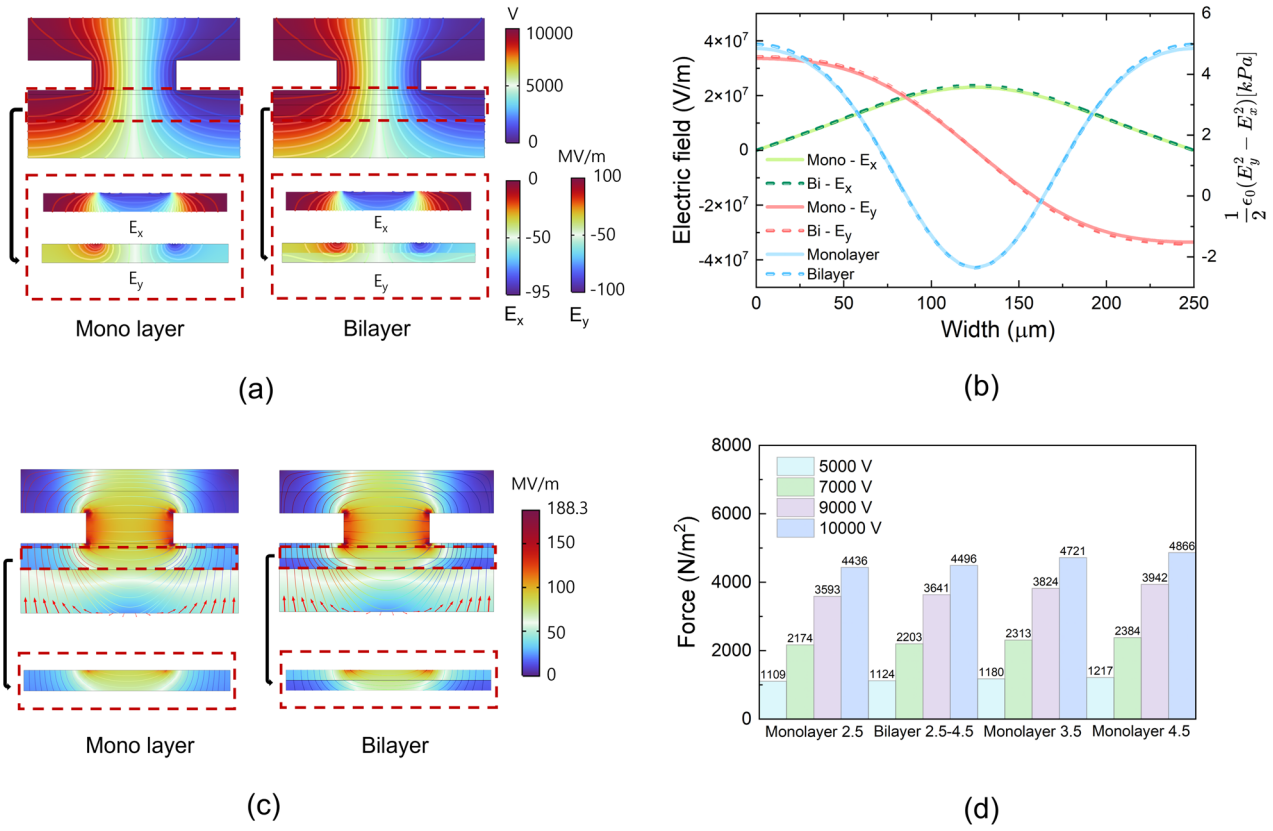

Figure 2. (**a**) Contour plots of the electrode potentials and potentials gradient according to the x and y-direction under an applied voltage of 10 kV. (**b**) Electrostatic field and maxwell stress tensor component measurements on the object surface. (**c**) Line profiles of the electrostatic field on the object surface and the corresponding Maxwell stress. (**d**) Calculated electrostatic force densities of the monolayer (ε_m= 2.5, 3.5, and 4.5) and bilayer (ε_{in}= 2.5 and ε_{out}= 4.5).

linear relationship between the applied voltage and the electrostatic adhesive force, wherein higher permittivity results in a greater electrostatic force. Note that, the analysis shows that a bilayer structure with inner and outer permittivities of 2.5 and 4.5, respectively, slightly improves the electrostatic force.

Random forest and sensitivity analysis

Figure 3a shows that increasing the permittivity of the monolayer configuration is an effective method for enhancing the electrostatic force. However, when selecting materials for the protective layer, it is essential to consider the operational voltage requirements, particularly the breakdown voltage[51]. Therefore, a bilayer design with low internal and external permittivities should be carefully considered. As the permittivity of the protective monolayer increases from 1 to 3, the electrostatic force exerted on the object surface increases steadily; however, it plateaus at higher permittivity levels. This suggests that although a higher permittivity can facilitate greater electric field penetration and increase the electrostatic force, this effect is limited. Notably, the permittivity variation within the protective layer results in a nonlinear electric field distribution, underscoring the complex relationship between material properties and electrostatic phenomena.

Recently, there has been a growing interest in using data-centric approaches with machine learning and artificial intelligence to optimize design parameters. Our electroadhesive gripper system has up to 8 parameters influencing its electroadhesive force. Conventional optimization methods, such as Levenberg–Marquardt, nonlinear least squares, and Newton–Raphson, can lead to inaccuracies due to missing local minima or other reasons, which take significant time to calculate. To optimize the design parameters that significantly affect the electroadhesive force of a bilayer protective structure, we performed a sensitivity analysis using the random forest (RF) algorithm on the results of 10,000 cases. To derive the 10,000 samples, we used a simulation with random values of parameters between their minimum and maximum values. We also tested several machine learning (ML) algorithms, including k-nearest neighbor, kernel ridge, support vector, and random forest regressions (RFR)[52–54]. The RFR algorithm most accurately fit the training data, as evidenced by the 500 sample points shown in Fig. 3b. Feature importance was automatically derived from the RF model (Fig. 3c). The results revealed that the applied voltage was the most influential design parameter for determining the electroadhesive force, underscoring the critical significance of the breakdown voltage of the protective layer. The air gap between the protective layer and the object emerged as the second most significant design parameter. This gap was maintained at 50 μm to optimize computational efficiency as it is an integral part of the actuator geometry. The protective layer permittivity, which was the primary focus of this study, exhibited the lowest sensitivity in response, with the permittivity of the inner layer being marginally more sensitive than that of the outer layer. Previous research on the protective layer of bilayer protective structures did not fully consider the influence of its dielectric constant owing to its low sensitivity[30]. Additionally, the possibility that the electrostatic force differs from previous findings was not considered either. This study acknowledged these omissions and aimed to address them. The findings of this study can provide valuable insights into the design parameters that significantly affect the electroadhesive force in bilayer protective structures.

Effect of design parameters on the force to object

Figure 4a,b show results of the electrostatic forces with respect to the permittivity of the bilayer. They indicate that the general electrostatic forces strengthen as bilayer permittivity increases. The permittivity of the inner layer was kept constant at 2.5, 3.5, and 4.5, whereas that of the outer layer was varied. Figure 4c indicates that the electrostatic forces reached their maximum values at the specific permittivity levels of the outer layer. These findings demonstrate the influence of the bilayer permittivity on the behavior of the electrostatic forces in a material. When the dielectric constant of the internal layer was set to 2.5, it was observed that the highest electroadhesive force of 4505 N/m^2 was obtained by using an outer layer permittivity of 3.8. However, it is important to note that the electroadhesive force may vary by up to 15.7%, resulting in a difference of 702.49 N/m^2 from the

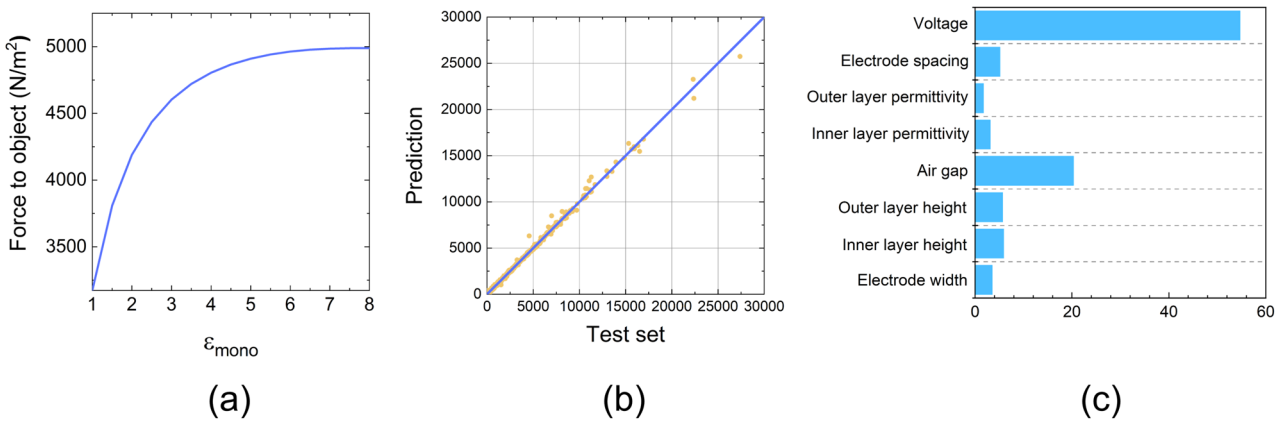

Figure 3. (**a**) Force per unit area applied to the object according to the permittivity difference in the monolayer structure. (**b**) Predicted electrostatic force values obtained using an ML algorithm (random forest (RF)). (**c**) Sensitivity analysis of the design parameters of RF. The intensity values of the sensitivity analysis are depicted using arbitrary units.

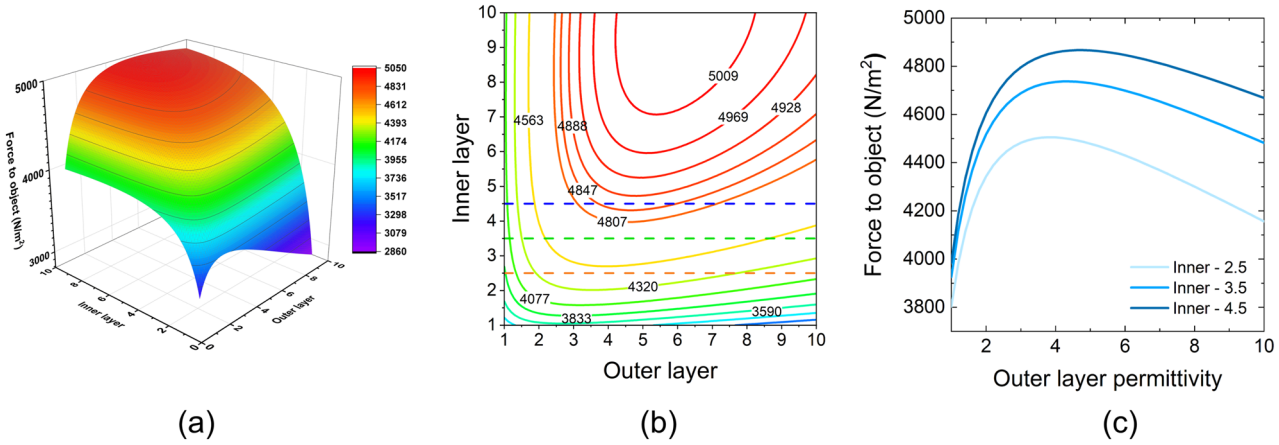

Figure 4. Calculation of electrostatic force according to the permittivities of the bilayer protective layers. (**a**) 3D representation of the effects of inner and outer layer thicknesses on the adhesive force. (**b**) Contour map illustrating the optimal layer thickness for specific electrostatic forces. (**c**) Line graph indicating the effects of outer layer permittivity on electrostatic force and changes in inner layer thickness on this relationship.

minimum value. As a result, it is advisable to optimize the dielectric constant when developing the bilayer. It is worth mentioning that this trend is more evident when the permittivity of the inner layer is increased. When the permittivity of 3.5 and 4.5 for the inner layer, the differences between the maximum and minimum forces reach 811.83 N/m^2 and 882.33 N/m^2 with permittivity of 4.4 and 4.8, respectively. This finding contradicts the previous assumption that a higher permittivity of the outer protective layer results in greater electrostatic forces.

Figure 5 shows that the electrostatic forces vary with the fixed bilayer protective layers as a function of the geometry of the interdigit electrode and the voltage applied to the electrode. In Fig. 5a, as the applied voltage increases, the adhesive force increases exponentially, which implies that the lifting force can be enhanced if the inner protective layer can sustain the applied voltage. Furthermore, decreasing the thickness of the protective layers and reducing the air gap between the objects and the outer protective layer can increase the attractive forces generated by applying a higher voltage, as shown in Fig. 5b,c. These results agree well with those reported by Liu et al., Mao et al., Guo et al., and Cao et al.[14,16,55,56]. As reported by Guo et al., to increase the electrostatic force, the spacing between the gap and the thick layers should be minimized[14]. However, a slightly different trend can be observed in the interdigit electrode width and spacing compared with the previous results, indicating that the spacing change between the electrodes generates the maximum attraction force. Figure 5d,e show that an optimum electrode width of 220 µm results in the maximum attraction force per unit area when the pad is attached to non-conductive substrates, wherein the space between the electrodes is fixed at 70 µm (optimum width/space ratio of 3.14).

Figure 6a,b illustrate the correlation between the geometry of the electrode and the electrostatic force. The electroadhesive force is calculated by considering the thickness of the protective layer and the distance between the electrodes (spacing), while the width of the electrode varies from 75 to 1000 µm. Specifically, the change in electrode width occurs simultaneously from both sides while moving in the out-plane direction of the electrode while maintaining the electrode spacing. The results indicate that the electrostatic force increases with electrode width up to a certain point, which indicates the optimal width at which the force is maximized. For thinner protective layers, such as 25 µm thickness, a more pronounced peak force is observed with an electrode width of 100 µm, while the maximum force is observed at 420 µm with the 500 µm thickness of protective layer. This result means that the optimum electrode width is dependent on the protective layer thickness. This suggests that a smaller distance between the electrode and the object enhances the electroadhesion efficiency. Moreover, the proximity of the electrodes also plays a crucial role. At a spacing of 50 µm, the most substantial force is induced with an electrode width of 225 µm. However, this force wanes when the spacing exceeds a certain threshold. This decline could be attributed to fringing effects or the dilution of the electric field over a larger area, which reduces the effective adhesive contact. The curve levels off as the electrode spacing increases, reflecting a substantial decrease in the effectiveness of the electrostatic force due to the diminished electric field intensity between the electrodes. This finding emphasizes the need for optimizing electrode width and spacing to maximize the electroadhesion force. Therefore, while designing electroadhesive systems, the physical dimensions of the electrode and air gap as well as the electrostatic principles governing adhesion must be carefully considered. Although material permittivity is a critical parameter, the geometric configuration is equally important.

Conclusions

This study comprehensively analyzed the impact of electrode design parameters on the performance of bilayer electroadhesion actuators through electrostatic simulations. The findings underscored the significance of electrode geometry, specifically electrode width and spacing, and the permittivity of the protective bilayers for optimizing the electroadhesive forces. The electroadhesive force increased with the electrode width up to a certain point, suggesting an optimal width for maximum adhesion efficiency. The peak electrostatic force occurred with a narrow thin protective layer, indicating that the reduced distance between the electrode and the object enhanced

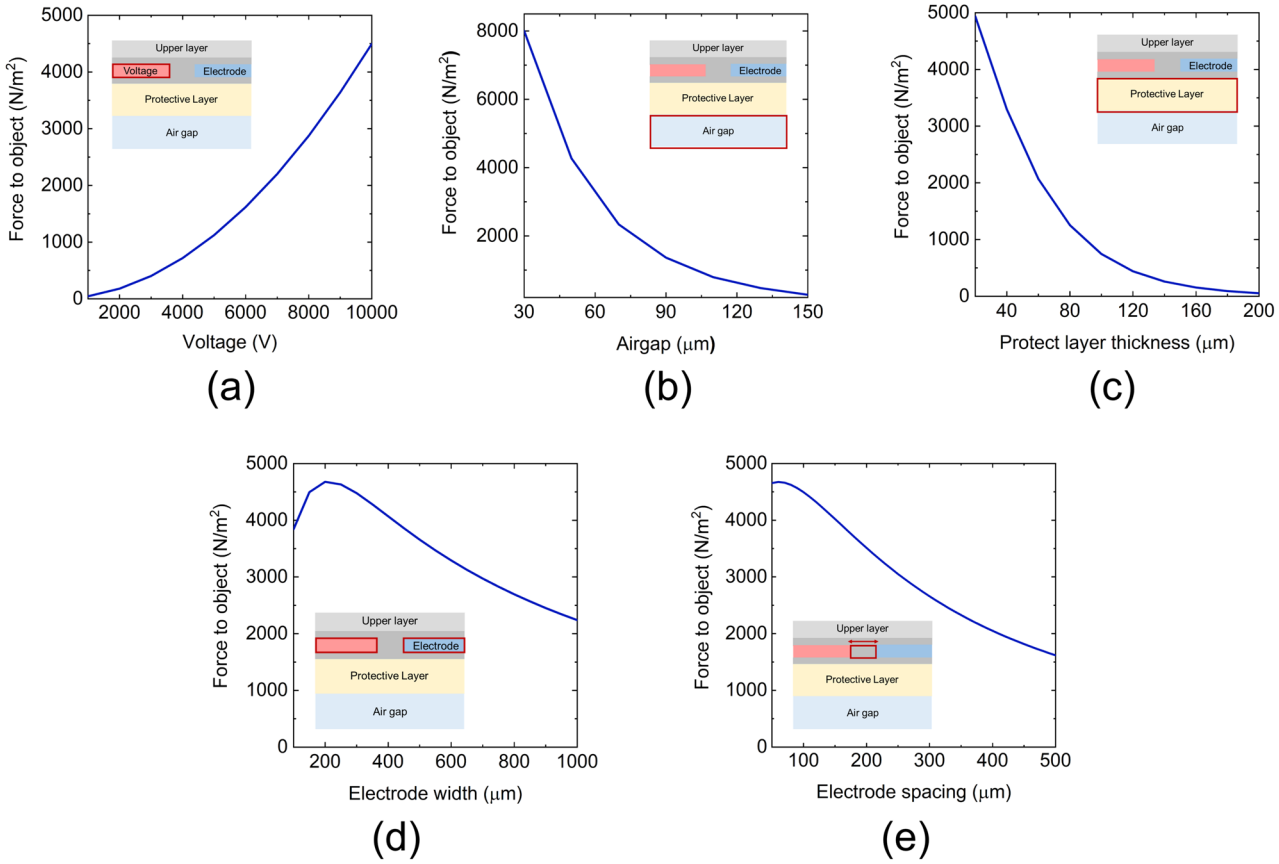

Figure 5. Electrostatic force calculations with various geometry design variables: (**a**) applied voltage, (**b**) air gap between the outer protective layer and the object, (**c**) protective layer thickness, (**d**) electrode width, and (**e**) electrode spacing.

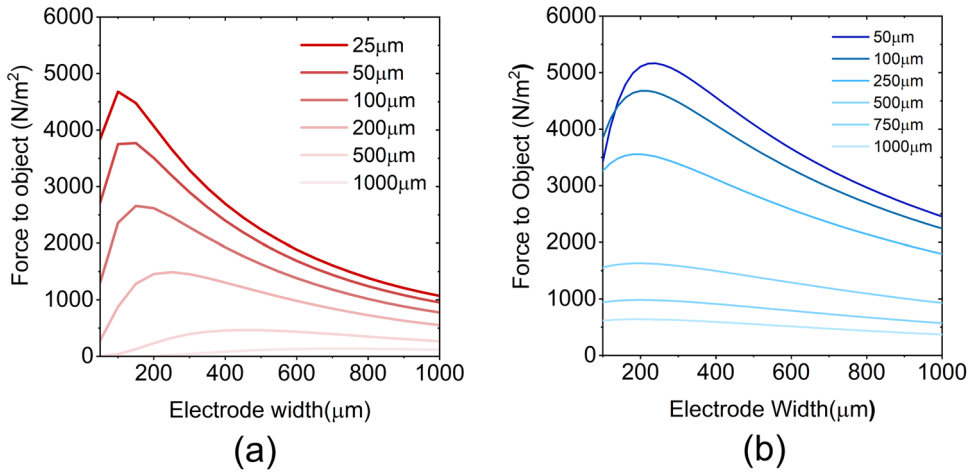

Figure 6. Varying the electrostatic force as a function of electrode width according to the (**a**) protective layer thickness (**b**) the gap between two electrodes (spacing).

electroadhesion. An optimal spacing of 50 μm between the electrodes substantially increased the induced force, demonstrating the importance of electrode geometry. Additionally, a larger electrode spacing diminished the electric field intensity and reduced the effectiveness of the force, emphasizing the need for careful geometric optimization. These insights can enhance the understanding of the physical principles governing electroadhesion and provide valuable guidance for designing more efficient and robust electroadhesive systems. Furthermore, the integration of ML algorithms enhanced the robustness of the analysis, offering predictive insights to guide the optimization of electroadhesive actuator behavior. Although the permittivity of materials is imperative, the

synergy between the material properties and geometric configuration of the actuator is critical to achieve peak performance. With carefully selected permittivity ratios, the bilayer design is a strategic approach for enhancing the electroadhesive force and ensuring that the operational voltage thresholds are met. Thus, the bilayer protective layer is a critical component, and its permittivity plays a decisive role in the modulation of electrostatic forces. This study established that, although the permittivity of each layer contributes to the overall performance, the relative permittivity between the layers can amplify or diminish the adhesion force. This nuanced understanding of the bilayer permittivity underscores its importance in the design and optimization of electroadhesive systems. Thus, by delving deeper into the effects of important design factors and work environments on the electroadhesion behavior, this study not only serves as a tool to clarify the basic principles of electroadhesion but also proposes prospective methods to enhance the design of electroadhesive devices for various engineering applications.

Data availability

All data generated or analyzed during this study are included in this published article and supplementary information S1.

Received: 15 February 2024; Accepted: 16 July 2024
Published online: 24 July 2024

References

1. Eshaghi, M., Ghasemi, M. & Khorshidi, K. Design, manufacturing and applications of small-scale magnetic soft robots. *Extreme Mech. Lett.* **44**, 101268 (2021).
2. Schaller, S. & Shea, H. Measuring electro-adhesion pressure before and after contact. *Sci. Rep.* **13**, 11768 (2023).
3. Xiang, C., Zhiwei, L., Wang, F., Guan, Y. & Zhou, W. A 3D printed flexible electroadhesion gripper. *Sens. Actuator A-Phys.* **363**, 114675 (2023).
4. Gao, D. *et al.* A supramolecular gel-elastomer system for soft iontronic adhesives. *Nat. Commun.* **14**, 1990 (2023).
5. Xiang, C., Guan, Y., Zhu, H., Lin, S. & Song, Y. All 3D printed ready-to-use flexible electroadhesion pads. *Sens. Actuator A-Phys.* **344**, 113747 (2022).
6. Cacucciolo, V., Shea, H. & Carbone, G. Peeling in electroadhesion soft grippers. *Extreme Mech. Lett.* **50**, 101529 (2021).
7. Chen, R. *et al.* Variable stiffness electroadhesion and compliant electroadhesive grippers. *Soft Robot.* **9**, 1074–1082 (2022).
8. Kim, D. G., Je, H., Hart, A. J. & Kim, S. Additive manufacturing of flexible 3D surface electrodes for electrostatic adhesion control and smart robotic gripping. *Friction* **11**, 1974–1986 (2023).
9. Nakamura, T. & Yamamoto, A. Modeling and control of electroadhesion force in DC voltage. *Robomech. J.* **4**, 18 (2017).
10. Guo, J., Leng, J. & Rossiter, J. Electroadhesion technologies for robotics: A comprehensive review. *IEEE Trans. Robot.* **36**, 313–327 (2020).
11. Cao, C., Gao, X., Guo, J. & Conn, A. De-electroadhesion of flexible and lightweight materials: An experimental study. *Appl. Sci.* **9**, 2796 (2019).
12. Guo, J. *et al.* Soft pneumatic grippers embedded with stretchable electroadhesion. *Smart Mater. Struct.* **27**, 055006 (2018).
13. Zhaojia, S., Wang, S., Zhao, Y., Zhong, Z. & Zuo, L. Discriminating soft actuators' thermal stimuli and mechanical deformation by hydrogel sensors and machine learning. *Adv. Intell. Syst.* **4**, 2200089 (2022).
14. Guo, J., Bamber, T., Chamberlain, M., Justham, L. & Jackson, M. Optimization and experimental verification of coplanar interdigital electroadhesives. *J. Phys. D-Appl. Phys.* **49**, 415304 (2016).
15. Choi, K. *et al.* Quantitative electrode design modeling of an electroadhesive lifting device based on the localized charge distribution and interfacial polarization of different objects. *ACS Omega* **4**, 7994–8000 (2019).
16. Cao, C. *et al.* Theoretical model and design of electroadhesive pad with interdigitated electrodes. *Mater. Des.* **89**, 485–491 (2016).
17. Guo, J., Hovell, T., Bamber, T., Petzing, J. & Justham, L. Symmetrical electroadhesives independent of different interfacial surface conditions. *Appl. Phys. Lett.* **111**, 221603 (2017).
18. Mici, J., Ko, J. W., West, J., Jaquith, J., Lipson. Parallel electrostatic grippers for layered assembly. *Addit. Manuf.* **27**, 451–460 (2019).
19. West, J. D., Mici, J., Jaquith, J. F. & Lipson, H. Design and optimization of millimeter-scale electroadhesive grippers. *J. Phys. D-Appl. Phys.* **53**(43), 435302 (2020).
20. Li, J. *et al.* Asymmetric strategy for enhanced performance of flexible electroadhesive clutch. *Heliyon* **9**, e12938 (2023).
21. Yuan, Y. *et al.* On variable stiffness of flexible parallel electroadhesive structures. *Addit. Manuf.* **32**, 055004 (2023).
22. Chiavarella, M., Papangelo, A. A simplified theory of electroadhesion for rough interfaces. *Front. Mech. Eng.-Switzerland* **6**, 00027 (2020).
23. Luo, A., Zhao, R. R., Bassani, J. L., Hart, A. J. & Turner, K. T. The critical role of fracture in determining the adhesion strength of electroadhesives. *Extreme Mech. Lett.* **63**, 102062 (2023).
24. Rajagopalan, P. *et al.* Advancement of electroadhesion technology for intelligent and self-reliant robotic applications. *Adv. Intell. Syst.* **4**, 2200064 (2022).
25. Lim, H., Hwang, G., Kyung, K. & Kim, B. Improved electroadhesive force by using fumed alumina/PDMS composites. *Smart Mater. Struct.* **30**, 035007 (2021).
26. Fessl, J., Mach, F. & Navrátil, J. Design, fabrication and testing of electroadhesive interdigital electrodes. *Open Phys.* **16**, 430–434 (2018).
27. Deepak Rosario, J. *et al*. Synergistic effect of impure/pure graphene oxide and TiO2 fillers on the dielectric properties of poly (vinylidene fluoride-hexafluoropropylene) for electroadhesive high load bearing applications. *J. Electroceram.* **50**, 23–36 (2023).
28. Deepak Rosario, J. *et al*. Influence of h-BN concentration on the development of PVDF-HFP/TiO2/h-BN nanocomposite films for electroadhesive applications. *J. Electron. Mater.* **53**, 1058–1066 (2024).
29. Chen, A. S. & Bergbreiter, S. All-polymer electroadhesives to a basic friction model. *Smart Mater. Struct.* **26**, 025028 (2017).
30. Akherat, S. M. J. M., Karimi, M. A., Alizadehyazdi, V., Asalzadeh, S. & Spenko, M. A tunable dielectric to improve electrostatic adhesion in electrostatic/microstructured adhesives. *J. Electrost.* **97**, 58–70 (2019).
31. Hossain, M. M. Effect of humidity on the breakdown strength and diffusion characteristics of polymer film. *Bull. Mat. Sci.* **16**(6), 699–707 (1993).
32. Fimbel, A., Abensur, T., Le, M., Capsal, J. & Cottinet, P. Accurate electroadhesion force measurements of electrostrictive polymers: The case of high performance plasticized terpolymers. *Polymers* **14**, 24 (2022).
33. Koh, K. H., Sreekumar, M. & Ponnanmbalam, S. G. Experimental investigation of the effect of the driving voltage of an electroadhesion actuator. *Materials* **7**(7), 4963–4981 (2014).
34. Stockinger, T. *et al.* High porous, ultra-thin paper sensors—An option for successful sensor integration. *Sens. Actuator A-Phys.* **350**, 114098 (2023).

35. Sîrbu, I. *et al.* Electrostatic actuators with constant force at low power loss using matched dielectrics. *Nat. Electron.* **6**(11), 888–899 (2023).
36. Zhao, D. Y. *et al.* Temperature and humidity sensor based on MEMS technology. *AIP Adv.* **11**(8), 085126 (2021).
37. Chopra, V., Chudak, M., Hensel, R., Darhuber, A. A., & Arzt, E. Enhancing dry adhesion of polymeric micropatterns by electric fields. *ACS Appl. Mater. Interfaces* **12**(24), 27708–27716.
38. Guo, J. *et al.* Experimental study of a flexible and environmentally stable electroadhesive device. *Appl. Phys. Lett.* **111**, 251603 (2017).
39. Guo, J. *et al.* Investigation of relationship between interfacial electroadhesive force and surface texture. *J. Phys. D-Appl. Phys.* **49**(3), 035303 (2016).
40. Persson, B. N. J. & Guo, J. Electroadhesion for soft adhesive pads and robotics: theory and numerical results. *Soft Matter* **15**(40), 8032–8039 (2019).
41. Bigharaz, M., Shenkel, T. & Bingham, P. A. Increasing force generation in electroadhesive devices through modelling of novel electrode geometries. *J. Electrost.* **109**, 103540 (2021).
42. Kong, Y. & Yu, T. A deep neural network model using random forest to extract feature representation for gene expression data classification. *Sci. Rep.* **8**, 16477 (2018).
43. Hwang, G., Park, J., Cortes, D. S. D., Hyeon, K. & Kyung, K. Electroadhesion-based high-payload soft gripper with mechanically strengthened structure. *IEEE Trans. Ind. Electron.* **69**, 642–651 (2022).
44. Persson, B. N. J. General theory of electroadhesion. *J. Phys. Condes. Matter*, **33**, 435001 (2021).
45. Guo, J., Xiang, C. & Rossiter, J. Electrically controllable connection and power transfer by electroadhesion. *Smart Mater. Struct.* **28**, 105012 (2019).
46. Xu, L. *et al.* Giant voltage enhancement via triboelectric charge supplement channel for self-powered electroadhesion. *ACS Nano* **12**, 10262–10271 (2018).
47. Kalus, W., Lagi, Ł & Zygarlicki, J. Analysis of potential of raising forces acting on electroadhesive pads depending on polarization and supply parameter. *Energies* **14**, 2517 (2021).
48. Piskarev, Y. *et al.* A soft gripper with granular jamming and electroadhesive properties. *Adv. Intell. Syst.* **5**, 202200409 (2023).
49. Mastrangelo, M., Caruso, F., Carbone, G. & Cacucciolo, V. Electroadhesion zipping with soft grippers on curved objects. *Extreme Mech. Lett.* **61**, 101999 (2023).
50. Levine, D. J. *et al.* A low-voltage, high-force capacity electroadhesive clutch based on ionoelastomer heterojunctions. *Adv. Mater.* **35**, 2304455 (2023).
51. Wang, W. *et al.* Automated pipeline for superalloy data by text mining. *NPJ Comput. Mater.* **8**, 9 (2022).
52. Stocker, S., Csányi, G., Reuter, K. & Margra, J. T. Machine learning in chemical reaction space. *Nat. Commun.* **11**, 5505 (2020).
53. Ngoc, L. V., Huang, C. Y., Cassidy, C. J., Medrano, C. & Kadonaga, J. T. Identification of the human DPR core promoter element using machine learning. *Nature* **585**, 459–463 (2020).
54. Zhang, X. *et al.* Machine learning modeling based on microbial community for prediction of natural attenuation in groundwater. *Environ. Sci. Technol.* **57**, 21212–21223 (2023).
55. Liu, R., Liu, R., & Shen, H. Modeling and analysis of electric field and electrostatic adhesion force generated by interdigital electrodes for wall climbing robots. In *IEEE Int. Conf. on Intelligent Robots and Systems* pp 2327–32 (Tokyo, 3–7 November 2013).
56. Mao, J., Qin, L., Zhang, W., Xie, L. & Wang, W. Modeling and analysis of electrostatic adhesion force for climbing robot on dielectric wall materials. *Eur. Phys. J. Appl. Phys.* **69**, 11003 (2015).

Acknowledgements

This research was supported by the National Research Foundation of Korea (NRF) grants funded by the Korean government (MSIT) (NRF-2021R1C1C1008383 and NRF-2022M3H4A1A02076956). This research was also supported by the Chung-Ang University Graduate Research Scholarship Grants in 2023.

Author contributions

S.P. and H.C. conceptualized the study. J.K. and H.C. prepared and analyzed the data. S.P. prepared the figures. H.C., J.K., and J.M. contributed to the discussions. S.P. and J.M. wrote the first draft. Y.G, and J.M. helped secure the funding. Y.G. and J.M. contributed to revising the manuscript.

Competing interests

The authors declare no competing interests.

Additional information

Supplementary Information The online version contains supplementary material available at https://doi.org/10.1038/s41598-024-67805-0.

Correspondence and requests for materials should be addressed to Y.G. or J.M.